

Emerging roles of CCM genes during tumorigenesis with potential application as novel biomarkers across major types of cancers

JOHNATHAN ABOU-FADEL, YANCHUN QU, ELIAS M. GONZALEZ, MARK SMITH and JUN ZHANG

Department of Molecular and Translational Medicine (MTM),
Texas Tech University Health Science Center El Paso, El Paso, TX 79905, USA

Received August 29, 2019; Accepted February 14, 2020

DOI: 10.3892/or.2020.7550

Abstract. Cerebral cavernous malformations (CCMs) are microvascular anomalies in the brain that result in increased susceptibility to stroke. Three genes have been identified as causes of CCMs: cerebral cavernous malformations 1 [(CCM1) also termed Krev interaction trapped 1 (*KRIT1*)], cerebral cavernous malformation 2 [(CCM2) also termed *MGC4607*] and cerebral cavernous malformation 3 [(CCM3) also termed programmed cell death 10 (*PDCD10*)]. It has been demonstrated that both CCM1 and CCM3 bind to CCM2 to form a CCM signaling complex (CSC) with which to modulate multiple signaling cascades. CCM proteins have been reported to play major roles in microvascular angiogenesis in human and animal models. However, CCM proteins are ubiquitously expressed in all major tissues, suggesting an unseen broader role of the CSC in biogenesis. Recent evidence suggests the possible involvement of the CSC complex during tumorigenesis; however, studies concerning this aspect are limited. This is the first report to systematically investigate the expression patterns of CCM proteins in major human tumors using real-time quantitative PCR, RNA-fluorescence *in situ* hybridization, immunohistochemistry and multicolor immunofluorescence imaging. Our data demonstrated that differential expression patterns of the CSC complex are correlated with certain types and grades of major human cancers, indicating the potential application of CCM genes as

molecular biomarkers for clinical oncology. Our data strongly suggest that more efforts are needed to elucidate the role of the CSC complex in tumorigenesis, which may have enormous clinical potential for cancer diagnostic, prognostic and therapeutic applications.

Introduction

CCM proteins have been demonstrated to play major roles in microvascular angiogenesis in human and animal models (1-6), which is an essential step for cancer growth during tumorigenesis (5,6). Three genes have been identified as causes of CCMs: cerebral cavernous malformations 1 [(CCM1) also termed Krev interaction trapped 1 (*KRIT1*)], cerebral cavernous malformation 2 [(CCM2) also termed *MGC4607*] and cerebral cavernous malformation 3 [(CCM3) also termed programmed cell death 10 (*PDCD10*)]. It has been demonstrated that both CCM1 and CCM3 bind to CCM2 to form a CCM signaling complex (CSC) with which to modulate multiple signaling cascades. As one of three key components of the CSC, CCM3 was initially identified as a tumor-associated apoptotic protein (7) which directly interacts with CCM2 within the CSC complex (8,9), suggesting that the CSC complex may be involved in tumorigenesis. CCM1 is ubiquitously expressed in various cells and tissues (5,10); likewise, almost all expressed isoforms of CCM2 are ubiquitously expressed in various cells and tissues (11), providing additional evidence for the potential involvement of the CSC in diverse cellular events in health and diseases, including cancer.

Previous data have shown much higher relative RNA expression levels of the *CCM1* gene in all cancer cell lines, compared to normal primary cell lines (5). In fact, CCM1 was found to act as a potential tumor suppressor inhibited in several cultured cancer cell lines by miR-21 (12), one of the most over-expressed small RNAs in a variety of solid cancers, including breast, colon, melanoma, cervix, ovarian, lung, pancreas, prostate and stomach cancers (13). Likewise, deficiency of Ccm1 in a mouse model showed an increased appearance of adenoma associated with increased β -catenin-mediated signaling (14), further supporting the potential role of CCM1 in tumorigenesis. As a docking protein for both CCM1 and CCM3, CCM2 (isoform-100) has been reported to be upregulated in various cardiovascular conditions, indicating its role as a possible potent angiogenic factor (15). Furthermore,

Correspondence to: Professor Jun Zhang, Department of Molecular and Translational Medicine (MTM), Texas Tech University Health Science Center El Paso, 5001 El Paso Drive, El Paso, TX 79905, USA
E-mail: jun.zhang2000@gmail.com

Abbreviations: CCMs, cerebral cavernous malformations; CSC, CCM signaling complex; qPCR, real-time quantitative polymerase chain reaction; RNA-FISH, RNA-fluorescence *in situ* hybridization; HRP, horseradish peroxidase; DAB, 3,3'-diaminobenzidine detection system; IHC, immunohistochemistry; IF, immunofluorescence; ROI, regions of interest; GBM, glioblastoma

Key words: cerebral cavernous malformations, CCM signaling complex, tumorigenesis, biomarkers, cancer

higher relative RNA expression levels of multiple *CCM2* isoforms were also observed in all cancer cell lines, compared to normal primary cell lines (11), reinforcing the phenomena observed in *CCM1* (5). *CCM2* was found to be a key mediator of TrkA-dependent cell death in tumors, by coupling among TrkA signaling, caspase activation, and cell death. Depletion of *CCM2* in medulloblastoma or neuroblastoma cells was found to attenuate TrkA-dependent death (16), suggesting that *CCM2* is a distinctive type of tumor suppressor that modulates tyrosine kinase signaling (17). These data suggest that both *CCM1* and *CCM2* act as tumor suppressors during tumorigenesis. *CCM3*, initially identified as a tumor suppressor (7), has been extensively studied for its role in tumorigenesis. Downregulation of *CCM3* is associated with the activation of Akt signaling protein in glioblastoma (GBM), implicating its role in tumor proliferation and apoptosis, hyperangiogenesis and peritumoral edema in GBM (18). Knockdown of *CCM3* in GBM cells was found to promote tumor growth and increased tumor mass and led to a chemo-resistance of mice treated with temozolomide (19). In co-cultured human endothelial cells (ECs) and GBM cell lines (U87 and LN229), silencing of *CCM3* in ECs significantly promoted tumor cell proliferation, migration, adhesion, invasion and inhibited apoptosis; this suggests that loss of endothelial *CCM3* intercellularly activates neighboring GBM cells and promotes tumor growth, likely via a paracrine mechanism (20). It has been demonstrated that *CCM3* is a direct target of multiple microRNAs during tumorigenesis. *CCM3* is a direct target of miR-103 which downregulates *CCM3* expression by binding the *CCM3* 3'UTR (21); miR-103 can play dual roles as either an oncogene or a tumor-suppressor in various types of cancers. As an oncogene, it promotes colorectal cancer by inhibiting tumor suppressors (22), and promoting triple-negative breast cancer cells to migrate and invade by targeting OLFM4 (23). As a tumor suppressor, miR-103 targets the c-Myc activators c-Myb and DVL1 resulting in reduced c-Myc expression in leukemia. Enhancement of miR-103 inhibits proliferation and sensitizes hemopoietic tumor cells for glucocorticoid-induced apoptosis, suggesting miR-103 as a hopeful therapeutic target and a useful prognostic biomarker for hemopoietic tumor cells (24), as well as to identify primary lung tumors with metastatic capacity (25). Interestingly, since miR-103 inhibits *CCM3* expression, *CCM3* usually plays an opposing role as miR-103 in this dual regulatory relationship. In non-small cell lung cancer (NSCLC) cell line, A549, *CCM3* expression was found to be increased while miR-103 expression was decreased, demonstrating that miR-103 acts as a tumor suppressor while *CCM3* acts as an oncogene in NSCLC (26). A similar relationship between miR-103 and *CCM3* was also observed in prostate cancer (21). These data suggest the existence of an opposing relationship between miR-103 and *CCM3* as either an oncogene or tumor suppressor during tumorigenesis.

In summary, previous data suggest that all three CCM proteins are likely involved in tumorigenesis in various stages of different cancers with distinctive roles; however, lack of systematic study of the CSC complex in tumorigenesis hinders our understanding in this aspect. In this report, we firstly performed a systemic analysis of expression patterns of three CCM proteins in multiple human cancers at both transcriptional and translational levels, using real-time quantitative

polymerase chain reaction (qPCR), RNA-fluorescence *in situ* hybridization (RNA-FISH), western blot analysis, immunohistochemistry (IHC) and multicolor immunofluorescence (IF) imaging technologies. Our data demonstrate a complicated role of the CSC complex observed in multiple human cancers, with promising data for potential biomarker applications of CCM genes for clinical oncology.

Materials and methods

Real-time quantitative PCR analysis (qPCR) and fluorescence *in situ* hybridization (FISH). Real-time quantitative PCR analysis (qPCR). Expression of CCM genes at both the transcriptional and translational levels was confirmed through both qPCR and western blot analysis. Allele-specific real-time quantitative PCR (qPCR) assays were designed using boundary-spanning primer sets as previously described (11) and applied to quantify the RNA levels of the endogenously expressed *CCM2* isoforms using Power SYBR Green Master Mix with ViiA 7 Real-Time PCR system (Applied Biosystems). TissueScan™ Real-Time PCR panels (HMRT100, 103, CSRT502) with Human β -actin control primer set (Origene) were used to determine the endogenous expression levels of *CCM2* isoforms among the different tissues at the transcriptional level. The qPCR data were analyzed with DataAssist™ (ABI; Thermo Fisher Scientific, Inc.) and Rest 2009 software (Qiagen). The relative expression level ($2^{-\Delta CT}$) was calculated from all samples and normalized to reference gene (β -actin); fold change ($2^{-\Delta\Delta CT}$) comparison was conducted by being further normalized to control groups (27). All experiments were performed with triplicates as described previously (11).

RNA fluorescence *in situ* hybridization (RNA-FISH). For FISH assay, DIG-labelled antisense *CCM2* isoform RNA probes (DIG-RNA) were synthesized with our *CCM2* isoform constructs, using Riboprobe *in-vitro* Transcription Systems (Promega) in combination with DIG RNA Labeling kit (Roche). Purified DIG-RNA probes were diluted to 20 μ g/ml in hybridization buffer. Multiple tumor and corresponding normal frozen tissue microarrays (BioChain, Biomax) were fixed in 4% PFA followed by dehydration in 20% sucrose and permeabilized with proteinase K (2 μ g/ml). It was then pre-hybridized, and subsequently hybridized with 100-200 ng/ml DIG-RNA antisense probes from various *CCM2* isoforms at 65°C overnight with the sense probes being used as negative controls; and mounted for IF analysis according to the manufacturer's instructions (BioChain, Biomax). The images were analyzed with NIS-Elements software (Nikon).

Immunohistochemistry (IHC) and immunofluorescence (IF) of paired normal-tumor tissue sections and western blot analysis

Deparaffinization of paraffin-embedded tissue sections. Slides (individual sections as well as microarrays) purchased from various suppliers [(T6234700-5, T6235086-PP, T8235086-PP, T8235149-PP; BioChain), (BCN962a, CM481, LV8011a, EMC1021, UT243, T233, TE242; LM482, US Biomax) and (T8235086-PP, Amsbio)] were baked at 60°C for 2 h. Once cooled, the sections were washed in 3 changes of xylene for 5 min each, followed by 3-min sequential washes

in 100, 95, 90, 80 and 70% ethanol and then soaked in water before an antigen retrieval step.

Antigen retrieval. Tissue sections were submerged in 10 mM sodium citrate buffer ($\text{Na}_3\text{C}_6\text{H}_5\text{O}_7$, pH 6.0) containing 0.01% Triton X-100 and were maintained at 95–98°C using a hotplate. The solution was carefully monitored to ensure boiling did not occur, which could have dislodged the tissue sections from the slide. Tissues were kept in citrate buffer at 95–98°C for 30 min and then allowed to cool down to room temperature (RT) in buffer. After being cooled, the slides were incubated at 37°C in a 0.05% Pronase solution in PBS. The combined heat-induced and enzyme-induced antigen retrieval methods were combined to increase staining with multiple conjugated antibodies.

Blocking and antibody incubation. After antigen retrieval: a) [for horseradish peroxidase (HRP)/3,3'-diaminobenzidine (DAB) detection system], the slides were briefly incubated in hydrogen peroxide block (supplied with the AB 64261 HRP/DAB detection kit; Abcam) for 10 min and washed 2 times in buffer (PBS+0.2% Triton X-100). Protein block was added (supplied with the AB 64261 HRP/DAB detection kit) for 10 min at RT followed by 1 wash. The primary antibody was added (dilution, 1:200) and incubated overnight (O/N) at 4°C. The tissue was then washed 4 times in buffer. Biotinylated goat anti-polyvalent (supplied with the AB 64261 HRP/DAB detection kit) was added to the tissue and incubated for 10 min at RT followed by 4 washes. Streptavidin peroxidase (supplied with the AB 64261 HRP/DAB detection kit) was then added and incubated at RT for 10 min, followed by 4 washes. One drop of DAB chromogen was added to 50 drops of DAB substrate (supplied with the AB 64261 HRP/DAB detection kit) immediately prior to applying on the tissue and incubation was carried out for 10 min followed by 4 rinses. Primary antibodies were purchased and included anti-CCM2 (Novus Biologicals; cat. no. NBP1-86730), CCM1 (Santa Cruz Biotechnology; cat. no. sc-514371), CCM3 (Santa Cruz Biotechnology; cat. no. sc-514371), PAQR7 (Aviva Systems Biology; cat. no. OASG04641), α -actin (Santa Cruz Biotechnology; cat. no. sc-17829) and β -actin (Santa Cruz Biotechnology; cat. no. sc-8432) antibodies. b) (for the IF detection system) The slides were briefly incubated in PBS containing 0.2% Triton X-100 for 10 min at RT to permeabilize the sections after antigen retrieval. Following permeabilization, the sections were blocked with PBS buffer containing 5.0% BSA with 0.2% Triton X-100 for 2 h at RT. Tissue sections were restricted using a hydrophobic pen which allows for conservation of antibodies. CCM1-Alexafluor® 488 (dilution, 1:1,000) (Santa Cruz Biotechnology; cat. no. sc-514371) and CCM3-Alexa Fluor® 647 (dilution, 1:500) (Santa Cruz Biotechnology; cat. no. sc-514371) antibodies were combined into PBS buffer containing 2.0% BSA and 0.2% Triton X-100 and initial 500 μl was placed directly above the tissue for incubation for 1 h at RT in the dark. Following the 1-h incubation at RT, fresh 500 μl of antibody solution was placed directly above the tissue for incubation O/N at 4°C in the dark.

Counterstaining with hematoxylin for IHC and mounting/sealing. Cell nuclei were counterstained (useful for

visualizing and normalizing HRP/DAB quantification) using Harris Hematoxylin solution (Sigma-Aldrich; Merck KGaA). Briefly, the slides were soaked in solution for 2 min and rinsed under running tap water for 5 min. Tissue sections were further blued using Scott's tap water (Sigma-Aldrich; Merck KGaA) for 3 min. Slides were then dehydrated ending in xylene and ready to be mounted and sealed. The tissue was then mounted using xylene-based mounting media and allowed to sit for 1 h, before sealing with nail polish to cure O/N. Immunofluorescence slides were DAPI stained during the mounting/sealing process as the UltraCruz mounting media (Santa Cruz Biotechnology) used for IF slides contain DAPI. To allow efficient staining of DAPI, the slides should be allowed to rest O/N at 4°C in the dark before sealing with nail polish to cure O/N.

Imaging and quantification. Imaging was carried out using either a Nikon EclipseTi microscope with a color camera for IHC or a Nikon Eclipse Ti confocal microscope for IF images. Images were acquired using a 10X objective lens to ensure coverage of tissue rather than in-depth visualization of a small region. Quantification was conducted automatically using Elements Analysis software provided with a Nikon microscope for both applications. Threshold was defined and maintained throughout all images for each application to ensure no bias was applied to the data. Thresholds were applied to exclude low and high outliers. The red/brown color from the HRP/DAB reactivity with the CCM2 antibody was quantified and averaged between the red and green channel quantification, and the fluorescent images were quantified for CCM1 and CCM3 using wavelength channels 488 and 647 nm, respectively.

Western blot analysis and quantification. The relative expression levels of CCM proteins were measured using western blot (WB) analysis. Equal amounts, (20 μg) determined through BCA assay (Bio-Rad), of protein lysates of paired tumors and adjacent normal tissues from liver (CP565477, CP520741, CP520759, CP565745, OriGene; P8235149-PP, BioChain) and endometrial tissues (CP565394, CP565528, CP565532, CP565549; OriGene) in modified RIPA buffer (150 mM NaCl, 1% NP-40, 0.5% sodium deoxycholate, 50 mM Tris-HCl, pH 8.0, and protease inhibitors) were separated on 4–15% Criterion Precast TGX (Bio-Rad) SDS-PAGE (sodium dodecyl sulphate-polyacrylamide gel electrophoresis) gels, then transferred to PVDF membranes, and probed with corresponding antibodies. All WB antibodies are listed in the Tissue-staining and immunohistochemistry (IHC) section above, which were conjugated with either chemiluminescence fluorescence for protein band imaging. WB images were acquired and analyzed using a GE imager analyzer LAS-4000 (GE Healthcare Life Sciences).

Statistical analysis. One-way analysis of variance (ANOVA) was used to detect the differences in the mean values among the treatment groups. All pairwise multiple comparison procedures were analyzed using Tukey and Student's un-paired t-test to test the difference between each treatment. Plots and charts were constructed and produced by SigmaPlot 12.0 (Systat Software, Inc.) and GraphPad Prism 8 (GraphPad Software, Inc.).

Results

Altered transcription expression of CCM2 isoforms in tumorigenesis. In our previous research, the RNA expression levels of *CCM1* were examined in different human tissues by northern blot analysis (10) and multi-tissue panels with qPCR (5). *CCM1* was found to be nearly ubiquitously expressed in all major tissues, indicating the potentially diverse functions of *CCM1*. The relative expression of the *CCM1* gene in homogenous cell populations from selected cell lines was also examined by qPCR (5). We found that compared to other cell lines, there was a much higher relative RNA expression level of the *CCM1* gene in all cancer cell lines (5) and likewise, the same phenomena were also observed in the relative RNA expression levels of *CCM2* isoforms (11). These data lead us to propose a potential role of the CSC in tumorigenesis in various tissues (5,11). To validate our *in vitro* findings, we screened TissueScan Real-Time cDNA sets for human tumor panels which covered all major types of cancer by qPCR, and found that while endometrial tumors had significantly decreased RNA expression levels of *CCM1*, both liver and testis tumors had significantly increased RNA expression levels of *CCM1* compared to their normal controls (5), suggesting that *CCM1* might have opposing roles in certain types of cancer during tumorigenesis. To further strengthen our findings, in the present study, we examined the expression levels of multiple *CCM2* isoforms by screening the same human major-tumor tissue panels with qPCR analysis. Intriguingly, our data showed a similar pattern of altered expression in all newly identified *CCM2* isoforms. Our data demonstrated that multiple isoforms had altered gene expression in major cancer tissues at the RNA level in comparison to their adjacent normal tissues, as representatively illustrated in Fig. 1A, proposing the potential role of *CCM2* isoforms in tumorigenesis. Furthermore, almost half of the screened tumors with altered RNA expression of *CCM2* isoforms (44%) were found to be cancers in the reproductive system (endometrium, breast and testis) (Fig. 1A), suggesting a major role of *CCM2* isoforms in reproductive cancer. Our qPCR data of *CCM2* isoforms in major types of cancers were also visualized with RNA fluorescent *in situ* hybridization (RNA-FISH). We utilized RNA-FISH technology with a specific *CCM2* isoform, *CCM2-212*, as a representative probe to screen cancer tissues; our data showed that an altered RNA expression level of the *CCM2-212* isoform was associated with tumorigenesis of various types of cancers (left panel, Fig. 1B). The relative expression changes were significantly different between normal and tumor tissues and the overall difference was also highly statistically significant ($P < 0.001$) (right panel, Fig. 1B). FISH data further validated our qPCR results indicating the involvement of *CCM2* isoforms during tumorigenesis.

Screening the altered expression of CCM2 protein among major cancers. To correlate our RNA expression profiling data of the *CCM2* gene in cancers, we next examined the protein expression levels of total *CCM2* protein in paired cancer-normal tissue sections from 16 major tissues (triplicates with each cancer tissue pair) utilizing immunohistochemistry (IHC) applications with horseradish peroxidase (HRP), 3,3'-diaminobenzidine (DAB) detection system. Based on the

expression patterns of total *CCM2* proteins, we classified these cancers into three groups: i) *CCM2* proteins were uniformly expressed in both tumor and normal tissues, with no difference detected between cancer and normal sections (Table I and Fig. 2A). ii) *CCM2* proteins were uniformly expressed in tumor and normal tissue pairs, but there were significant differences in the *CCM2* protein expression levels between tumor and normal tissues. In this group, we identified several cancers defined with significantly altered expression of total *CCM2* protein (Table I and Fig. 2B-a-d). iii) *CCM2* protein was not uniformly expressed in tumor and normal tissue pairs, in which tumor samples usually had larger than usual variation (statistically larger standard deviations, SD) leading to no significant expression differences between tumor and normal tissues, classified here as a heterogeneous nature in this group of cancers (Table I and Fig. 2C-a-c).

Validation of the identified cancers with altered expression of CCM2 protein. To duplicate these findings (Table I and Fig. 2), we further investigated four major cancer tissue-pairs using different tissue panels with a much larger sample size ($n \geq 10$); one from group B (Table I, endometrium) and two from group C (Table I, testes and liver) with possible heterogeneous nature. No obvious differences were observed in testis paired-tumor tissues, which is represented by the section (left panel) and primary quantification of the specific tumor-pair (middle panel) and overall quantification of the entire collection (right panel) (Fig. 3A). This result may eliminate the possible involvement of *CCM2* in the testes during tumorigenesis. In agreement with our preliminary data (Table I and Fig. 2Bc), significant increases in total *CCM2* protein were consistently observed in endometrial tumors, which is represented by sections (left panel) and primary quantification of the specific tumor-pair (middle panel) and overall quantification of the entire collection (right panel) (Fig. 3B). Notably, our preliminary data showed two contradicting expression patterns of *CCM2* proteins in liver tumors (Table I and Fig. 2C-a), suggesting the heterogeneity of liver tumors. The larger cohort of liver cancer screening indicated that statistically significant increases in total *CCM2* protein were predominately observed in liver tumors, which is represented by the section (left panel) and primary quantification of the specific tumor-pair (middle panel) and overall quantification of the entire collection (right panel) (Fig. 3C).

Evaluation of the co-expression levels of CCM1 and CCM3 proteins among the identified cancers associated with altered CCM2 expression. To further elucidate the coordinated relationship among the three *CCM* proteins within the CSC complex in tumorigenesis, we next examined the protein co-expression levels of *CCM1* and *CCM3* proteins in identified human cancers associated with altered *CCM2* expression. Using endometrial tumor tissues consisting of three different stages of endometrial tumor (adenocarcinoma, T), grade 1 (T G1), grade 2 (T G2), grade 3 (T G3), and normal tissue (N), we examined the protein expression levels of *CCM1* and *CCM3* using multicolor immunofluorescence (IF) imaging among these stages of cancers. The coordinated increase in both *CCM1* and *CCM3* proteins were found in the different stages of endometrial tumor (adenocarcinoma, T), compared

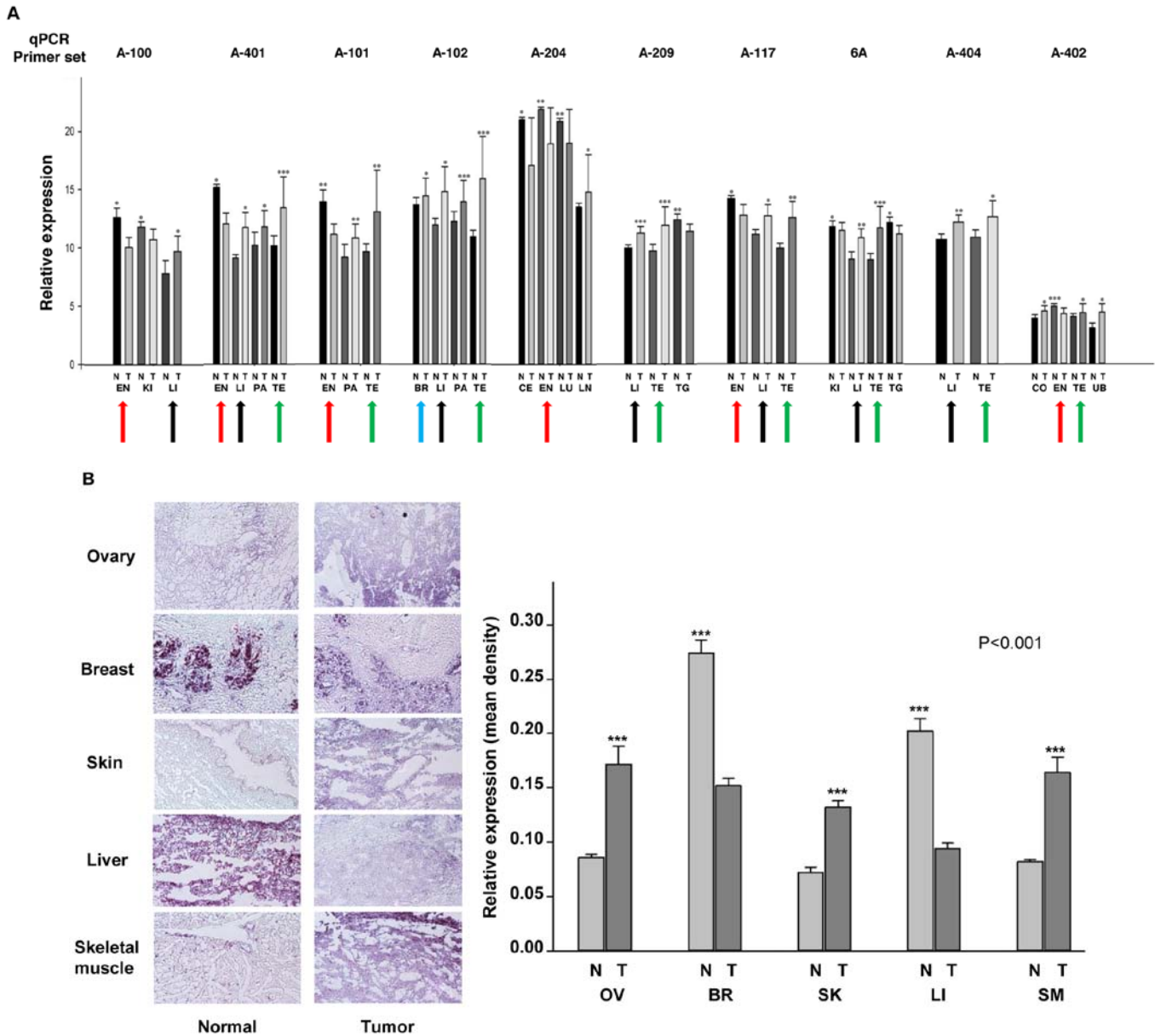


Figure 1. Altered RNA expression of CCM2 isoforms in major types of cancer. (A) Relative RNA expression levels of endogenous CCM2 isoforms in tumor tissues as measured by qPCR are presented as bar plots where the dark bars represent normal tissues (N) and light bars represent tumor tissues (T), among each tissue pair. Endometrium (EN) (red arrow), breast (BR) (blue arrow), testis (TE) (green arrow), and liver (LI) (black arrow) were observed as the most common tumor tissues with altered RNA expression among the CCM2 isoforms. Other tumor tissues tested included kidney (KI), pancreas (PA), cervix (CE), lung (LU), colon (CO), lymph node (LN), thyroid gland (TG) and urinary bladder (UB). The relative expression levels of endogenous CCM2 isoforms ($2^{-\Delta C_t}$) were calculated for each tissue pair. (***) $P \leq 0.001$, (**) $P \leq 0.01$ and (*) $P \leq 0.05$, respectively, for paired t-test, $n=3$.) (B) Significant expression changes of the CCM2 isoform, CCM2-212, in major tumor tissues. RNA expression changes of CCM2 isoform, CCM2-212, in certain tumor tissues were defined by RNA fluorescence *in situ* hybridization (RNA-FISH). Adjacent serial sections of normal (N) and tumor tissues (T) were hybridized with antisense probes from the CCM2-212 isoform. Five paired normal-tumor tissue panels, ovary (OV), breast (BR), skin (SK), liver (LI) and skeletal muscle (SM), demonstrated significant antisense FISH staining with the CCM2-212 isoform (left panel). The visual differences were further validated with quantitative comparison between normal and tumor tissues. The staining differences in the CCM2-212 isoform were quantified by densitometry, measured as mean density and normalized with background probe and adjacent normal tissues (right panel). One-way ANOVA was also performed for the comparison between normal and tumor tissues and it was found that there was a very significant difference for the expression levels of the CCM2-212 isoform in these five pairs of normal and tumor tissues (bars represent mean \pm SD, (***) $P \leq 0.001$ for paired t-test, $n=3$). CCM2, cerebral cavernous malformation 2.

to normal tissue (N) with significant differences and peak expression of CCM1 and CCM3 in grade 2 and grade 3 respectively (Fig. 4A-a and -b). The general consent is that the increased protein levels of CCM1 and CCM3 are associated with increased clinical severity of endometrial tumors, indicating a potential application of CCM proteins as diagnostic and prognostic biomarkers for endometrial cancers. Western

blot analysis further validated our IF imaging data; significantly increased protein levels of CCM1 and CCM3 were found in the endometrial tumors (T) when compared to that noted in the normal tissues (N) (Figs. 4A-c, S2A and B).

The expression levels of CCM1 and CCM3 proteins among various liver conditions [hepatitis, cirrhosis, grade1 liver tumor (T G1)], were also examined (Fig. 4B-a). Our IF imaging data

Table I. Classification of the major human cancers based on the expression level of the CCM2 protein.

Group	Tumor type	N	Mean	SD	Uniform	P-value
A	Esophageal squamous cell carcinoma				Y	
	Normal		0.9998	0.0803		
	Tumor	3	0.9349	0.0004		
	t-test					0.1170
	Prostate adenocarcinoma				Y	
	Normal	3	1.0000	0.0004		
	Tumor	3	0.9510	0.0461		
	t-test					0.0694
B	Stomach adenocarcinoma				Y	
	Normal	3	1.0000	0.0001		
	Tumor	3	0.8630	0.0570		
	t-test					0.0070 ^b
	Lung adenocarcinoma				Y	
	Normal	3	1.0000	0.0005		
	Tumor	3	1.0590	0.0353		
	t-test					0.0221 ^a
	Kidney clear cell carcinoma				Y	
	Normal	3	1.0000	0.0003		
	Tumor	3	0.9030	0.0736		
	t-test					0.0418 ^a
	Invasive ductal carcinoma (breast)				Y	
	Normal	3	0.9990	0.0002		
	Tumor	3	1.2060	0.0275		
	t-test					0.0001 ^v
	Cervical squamous cell carcinoma				Y	
	Normal	3	1.0000	0.0003		
Tumor	3	1.1580	0.0981			
t-test					0.0243 ^a	
Diffuse large B-cell lymphoma				Y		
Normal	3	1.0000	0.0013			
Tumor	3	0.8760	0.0521			
t-test					0.0074 ^v	
C	Colon mucinous adenocarcinoma				N	
	Normal	3	0.9990	0.0003		
	Tumor	3	0.9460	0.2110		
	t-test					0.3400
	Hepatocellular carcinoma				N	
	Normal	3	1.0000	0.0002		
	Tumor	3	0.9180	0.1780		
	t-test					0.2350
	Ovarian serous papillary adenocarcinoma				N	
	Normal	3	1.0000	0.0016		
	Tumor	3	1.0250	0.1050		
	t-test					0.3470
Urothelial carcinoma				N		
Normal	3	1.0000	0.0002			
Tumor	3	1.1410	0.1380			
t-test					0.0756	
Squamous cell carcinoma (skin)				N		
Normal	3	1.0000	0.0003			
Tumor	3	1.1930	0.1820			
t-test					0.0694	

Table I. Continued.

Group	Tumor type	N	Mean	SD	Uniform	P-value
	Pancreatic adenocarcinoma				N	
	Normal	3	1.0000	0.0005		
	Tumor	3	0.8960	0.1330		
	t-test					0.1240
	Testicular anaplasia seminoma				N	
	Normal	4	1.0010	0.0024		
	Tumor	4	1.0190	0.1060		
	t-test					0.3700

The relative expression levels of total endogenous cerebral cavernous malformation 2 (CCM2) protein in tumor and adjacent normal tissues were assessed by utilizing immunohistochemistry (IHC) applications with horseradish peroxidase (HRP), 3,3'-diaminobenzidine (DAB) detection system for each tissue-pair (tumor/normal). These tumor-normal pairs were classified into three groups based on both sample uniformity (Uniform) and statistical results: Group A, the tissue-pair was uniform and no difference in CCM2 expression was noted; group B, the tissue-pair was uniform but with differential expression levels for CCM2 proteins; group C, the tissue-pair was not uniform (the standard deviation of at least one of the samples was >0.1). The uniformity of each tissue-pair was reached (Y, yes) as the standard deviation (SD) of both tissue sections (tumor/normal) was simultaneously <0.1 . However, there was no uniformity between two sections (tumor/normal) if the standard deviation (SD) passed 0.1 (N, no). A total of 15 different tumor-normal pairs were qualified to be measured and statistically analyzed with three to four replicates for each tissue-pair ($^aP \leq 0.05$ and $^bP \leq 0.001$ significant differences for paired t-test, $n=3-4$).

indicated that altered expression patterns of both CCM1 and CCM3 proteins were observed in the three different stages of liver disease (Fig. 4B-a). However, the expression patterns of both CCM1 and CCM3 proteins were more complicated than that noted in endometrial cancers. Increased expression levels of CCM3 proteins at the earlier stages of liver tumorigenesis (cirrhosis and hepatitis) were observed, while increased expression levels of CCM1 were seen only in cirrhosis tissue. Interestingly, CCM1 and CCM3 were significantly decreased in stage-1 liver tumors when compared to that found in the normal tissue (Fig. 4B-b). These data suggest that expression patterns of both CCM1 and CCM3 proteins are very heterogeneous. Interestingly, western blot analysis with protein lysates from different suppliers showed significantly increased protein levels of both CCM1 and CCM3 in liver tumors (T), compared to that in normal tissues (N) (Figs. 4B-c and S2A and B), validating the heterogeneous nature of CCM1 and CCM3 expression in various liver conditions.

Confirmation of CCM protein-associated cancers with a validated tumor marker. The progesterin and adipoQ receptor 7 (PAQR7) has been found to be highly expressed in mammalian reproductive tissues, especially in female ovaries (28). Evidence has shown that PAQR7 is abundantly expressed in ovarian cancer cells (29), and altered expression of PAQR7 has been observed in ovarian tumors at both the messenger RNA and protein levels (30), making it a valuable candidate as a positive control to examine gene expression levels in endometrial tumors. Therefore, we firstly examined the protein expression levels of PAQR7 in paired endometrial tumor (adenocarcinoma) (T) and normal (N) tissues. In accordance with previous research (30), significant increased expression levels of PAQR7 protein were observed in endometrial tumors (Fig. 5A, left panel). The expression difference between endometrial tumors and normal adjacent endometrium showed marked differences in both

the representative quantification of the specific tumor-pair (Fig. 5A, middle panel) and overall quantification of the entire collection (Fig. 5A, right panel). However, the significantly high variations noted among the entire collection suggest the heterogeneity of endometrial tumors (Fig. 5A, right panel). To resolve this issue, we further stratified this endometrial tumor collection into two categories: grade 1 and grade 2-2/3. Upon this reclassification, a significantly increased expression level of PAQR7 protein was observed in grade 1 endometrial tumors, which is represented by the tissue section (Fig. 5B, left panel) and both the representative quantification of the specific tumor-tissue pair (Fig. 5B, middle panel) and overall quantification of the entire grade 1 tumors (Fig. 5B, right panel). Further significantly increased expression levels of PAQR7 protein were observed in grade 2-2/3 endometrial tumors, which is represented by the tissue section (Fig. 5C, left panel) and both the representative quantification of the specific tumor-tissue pair (Fig. 5C, middle panel) and overall quantification of this category (Fig. 5C, right panel). Interestingly, this increased expression pattern of PAQR7 protein observed for grade 1 and 2-2/3 is somewhat in parallel to the similar trend of the expression levels of CCM1 and CCM3 proteins observed in endometrial cancers (Fig. 4A), suggesting a possible correlation of expression among CCM proteins and PAQR7 in endometrial cancers. We then examined the expression pattern of PAQR7 protein in liver tumors, revealing an opposite trend of PAQR7 expression observed in endometrial cancers. PAQR7 expression was markedly downregulated in the liver tumor tissue, which is represented by the tissue section (Fig. 5D, left panel) and both the representative quantification of the specific tumor-tissue pair (Fig. 5D, middle panel) and overall quantification of the entire collection (Fig. 5D, right panel).

Consistently increased expression of CCM2 protein in heterogeneous lymphoma. Although a quite homogenous expression

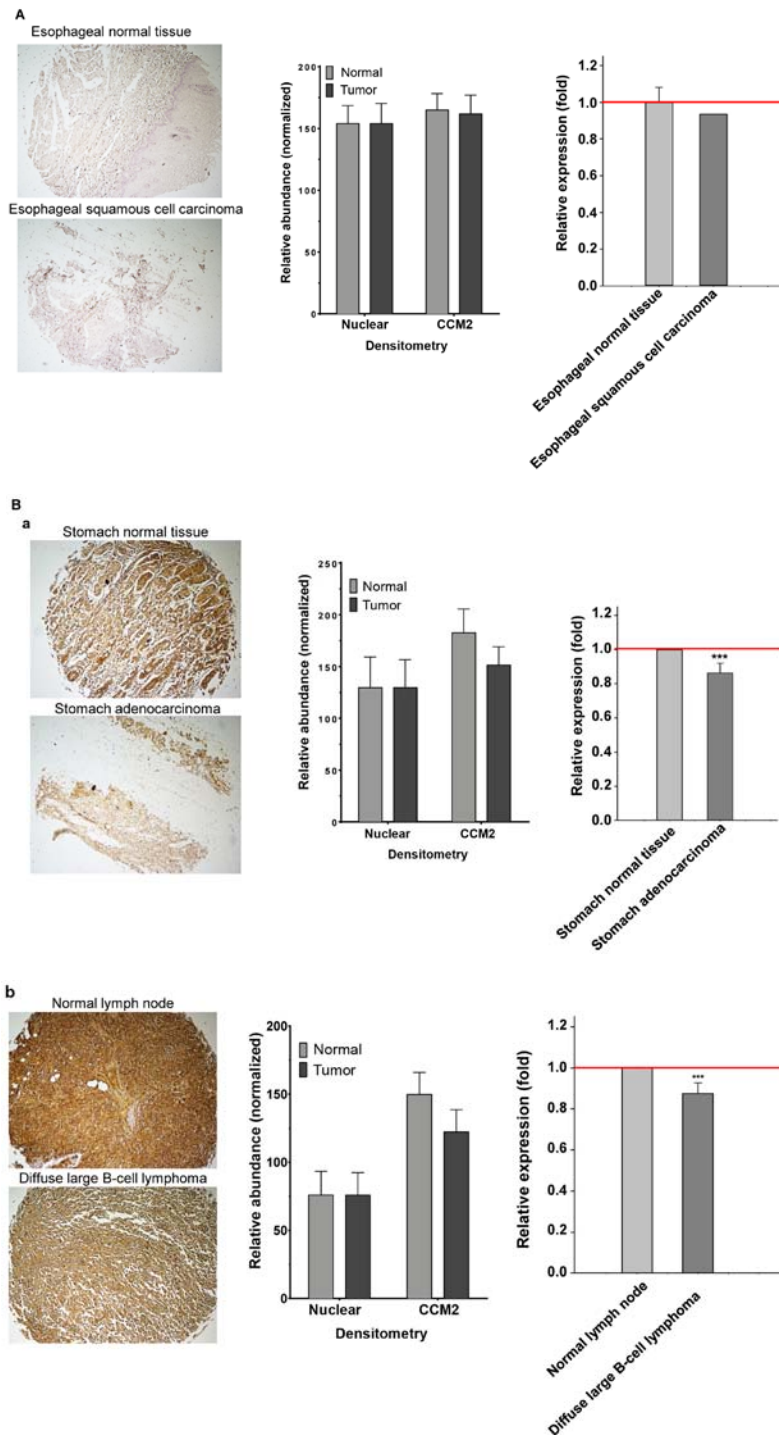


Figure 2. Major human cancer is classified into three classes based on their expression patterns of total CCM2 protein. The relative expression of total CCM2 protein in various types of tumors (tumor) comparing to adjacent normal tissue (normal) in the format of paired-tissue samples were examined. Tumors derived from 16 different major human tissues were probed on a single tumor array (BCN962a, Biomax) with the CCM2 antibody utilizing immunohistochemistry (IHC) applications with horseradish peroxidase (HRP), 3,3'-diaminobenzidine (DAB) detection system and quantified with Elements Analysis software. The red/brown color from HRP/DAB reactivity with the CCM2 antibody was quantified and averaged between the red and green channel quantification and cell nuclei were quantified with the blue channel. Data were normalized against the respective internal controls using the blue channel for cell nuclei and background staining. Relative densitometry and relative expression of total CCM2 proteins are presented as bar plots where the light bars represent normal tissues and dark bars represent tumor tissues among each tissue pair. Three groups were defined among these tumor-normal pairs (Table I). (A) The tissue-pair is uniform, and no statistical difference was found for CCM2 expression. In the representative esophageal section, although there may be some subtle morphological changes observed, no visual difference in the relative intensity of CCM2 staining was identified between the tumor (squamous cell carcinoma) and normal tissues in the esophageal tissues-pair from DAB staining (left panel); no statistical difference was found through the quantification of the relative expression level of CCM2 for the representative pair (ROI, normal=5,641, tumor=2,500) (middle panel), and no statistical difference was found through the overall quantification of the relative expression level of CCM2 between tumor (carcinoma) and normal esophageal tissues (n=3) (right panel). (B) The tissue-pair was uniform but with different expression levels of CCM2 protein. In the representative sections from four locations, compared to their adjacent normal control tissues, there were significant visual decreases in the relative intensity of CCM2 staining in the representative sections of (a) stomach adenocarcinoma (ROI, normal=8,715, tumor=5,308) and (b) diffuse large B-cell lymphoma (ROI, normal=15,168, tumor=7,605), while significant visual increases in the relative intensity of CCM2 staining in the representative sections of (c) cervical squamous cell carcinoma (ROI, normal=8,674, tumor=8,672) and (d) breast invasive ductal carcinoma (ROI, normal=9,739, tumor=5,913) were observed (middle panels).

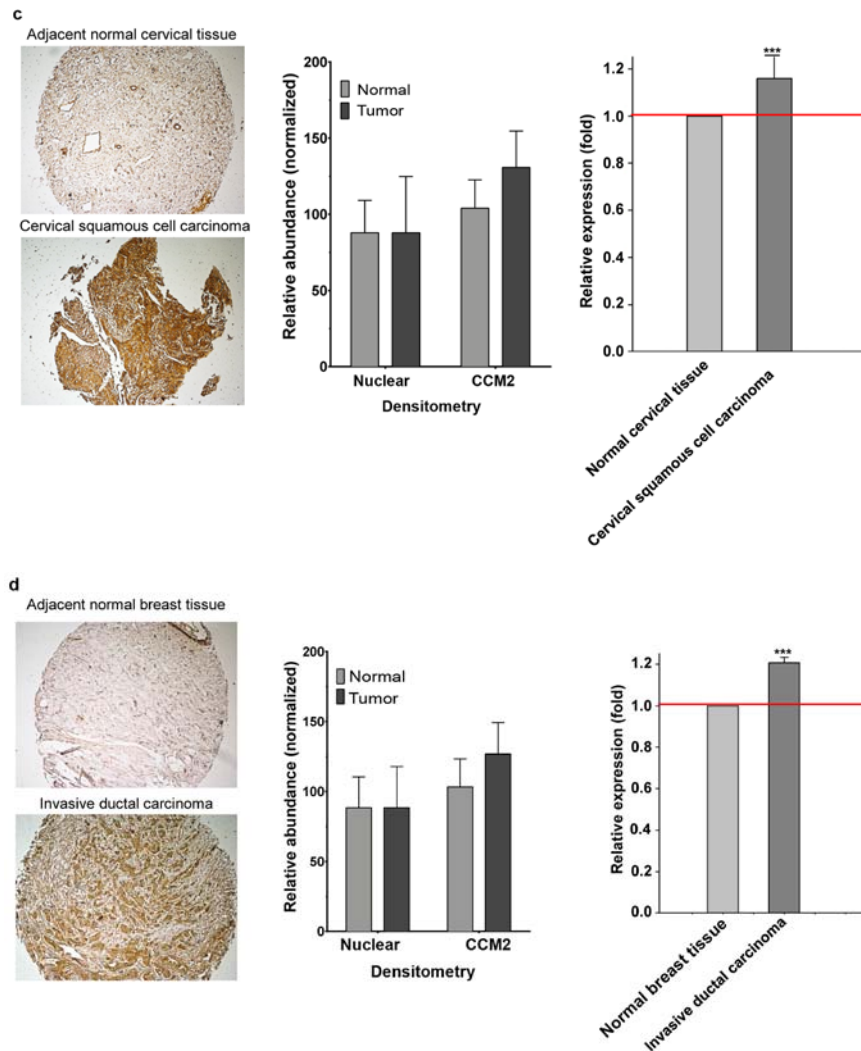


Figure 2. Continued. (B) The tissue-pair was uniform but with different expression levels of CCM2 protein. In the representative sections from four locations, compared to their adjacent normal control tissues, there were significant visual decreases in the relative intensity of CCM2 staining in the representative sections of (a) stomach adenocarcinoma (ROI, normal=8,715, tumor=5,308) and (b) diffuse large B-cell lymphoma (ROI, normal=15,168, tumor=7,605), while significant visual increases in the relative intensity of CCM2 staining in the representative sections of (c) cervical squamous cell carcinoma (ROI, normal=8,674, tumor=8,672) and (d) breast invasive ductal carcinoma (ROI, normal=9,739, tumor=5,913) were observed (middle panels). These significant differences were confirmed through the quantification of the relative expression levels of CCM2 between tumor and normal tissues (n=3) (right panels) (***) $P \leq 0.001$ for unpaired t-test depending on tissue sample being quantified).

pattern was observed in diffuse large B-cell lymphoma (Table I and Fig. 2), generally, lymphomas are collections of a heterogeneous group of tumors in lymph nodes located in various tissues. We explored the expression pattern of CCM2 proteins in a collective group of lymphomas from 43 tissue sections at various body locations (Figs. 6 and S1A-D); notably, an apparent trend of increased expression levels of CCM2 proteins were observed in various lymphomas in the neck (Figs. 6A and S1C and groin (Fig. 6B), suggesting that CCM2 potentially is a novel biomarker across various lymphomas in the neck and groin.

Expression patterns of CCM2 among plasma cell myeloma in the clavicle, sternum, thoracic vertebrae and pubis (Figs. 6C and S1A) also demonstrated increased expression regardless of location. We also observed a similar trend of increased CCM2 expression among plasma cell myeloma in various ribs, while plasma cell myeloma of the third rib was the only sample to display a slight decrease compared

to normal tissue (Fig. S1B). A similar trend of increased CCM2 expression patterns was noted in diffuse large B-cell lymphomas of various organs (Figs. 6D and S1C) and in follicular non-Hodgkin's lymphoma in various locations (Fig. S1D). Finally, we also observed a similar trend in CCM2 expression among diffuse T-cell lymphoma in the knee and nose, while interestingly, a very slight decrease was observed for T-cell lymphoma of the mediastinum, which was the only lymph cancer tissue sample in this group to display a slight decrease in CCM2 expression (Fig. 6E, left and right panels). In summary, upon combination of the 43 tissue sections of various lymphomas at various body locations (Figs. 6A-E and S1A-D), a pattern of increased expression levels of CCM2 proteins were clearly demonstrated for various lymphomas, even with the two samples that displayed decreased CCM2 expression (Fig. 6F), suggesting CCM2 protein as a potential biomarker for lymphoma diagnostic and prognostic applications. Further efforts will be made to

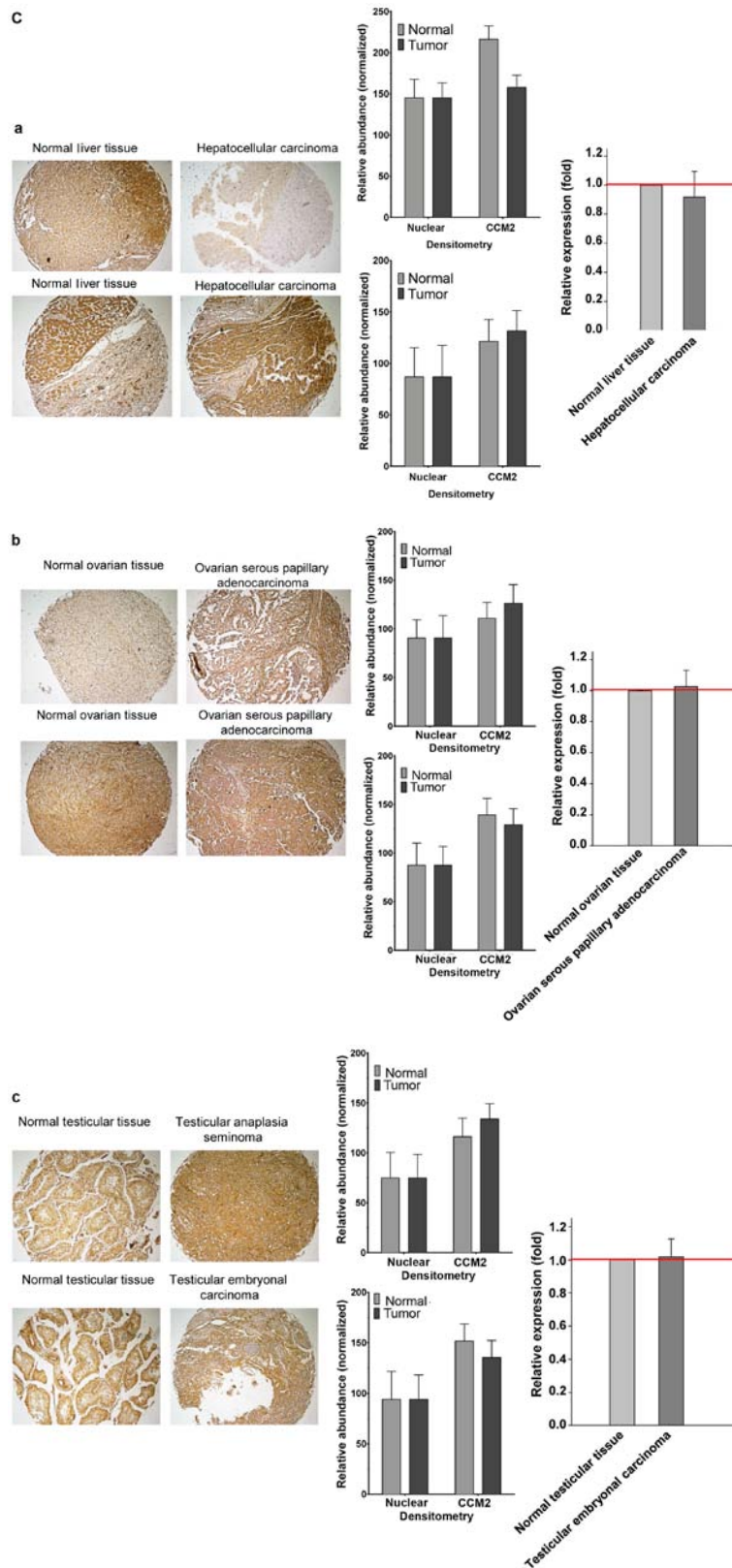


Figure 2. Continued. (C) The tissue-pair is not uniform. Significant variation was found among tissue-pairs. In the representative sections from three locations, compared to their adjacent normal control tissues, contradictory and significant increase and decrease (upper and lower left panels) were simultaneously observed in the relative intensity of CCM2 staining in either (a) hepatocellular carcinoma (ROI in increased expression, normal=13,782, tumor=5,765; ROI in decreased expression, normal=9,961, tumor=9,555) (middle panels), (b) ovarian serous papillary adenocarcinoma (ROI in increased expression, normal=10,460, tumor=7,750; ROI in decreased expression, normal=9,056, tumor=10,806) (middle panels) or (c) testicular anaplasia seminoma (ROI in increased expression, normal=6,752, tumor=10,288; ROI in decreased expression, normal=8,219, tumor=8,503) (middle panels), which resulted in no differences detected in the quantification of the relative expression level of CCM2 between tumor and normal tissues (n=3,4) (right panels). Automated quantification of regions of interest (ROI) intensities of CCM2 protein was accomplished with Elements Analysis software. Graph for the representative sections is determined by the quantification obtained of the >2,500 observations (ROI). The relative expression levels of endogenous CCM2 protein are presented with bar plots which was normalized against normal tissue cell nuclear staining among each tissue pair (middle panels) and further normalized against normal tissue for the entire collection (right panels). Red line on quantification graphs represents baseline for the normalized control. CCM2, cerebral cavernous malformation 2; ROI, regions of interest.

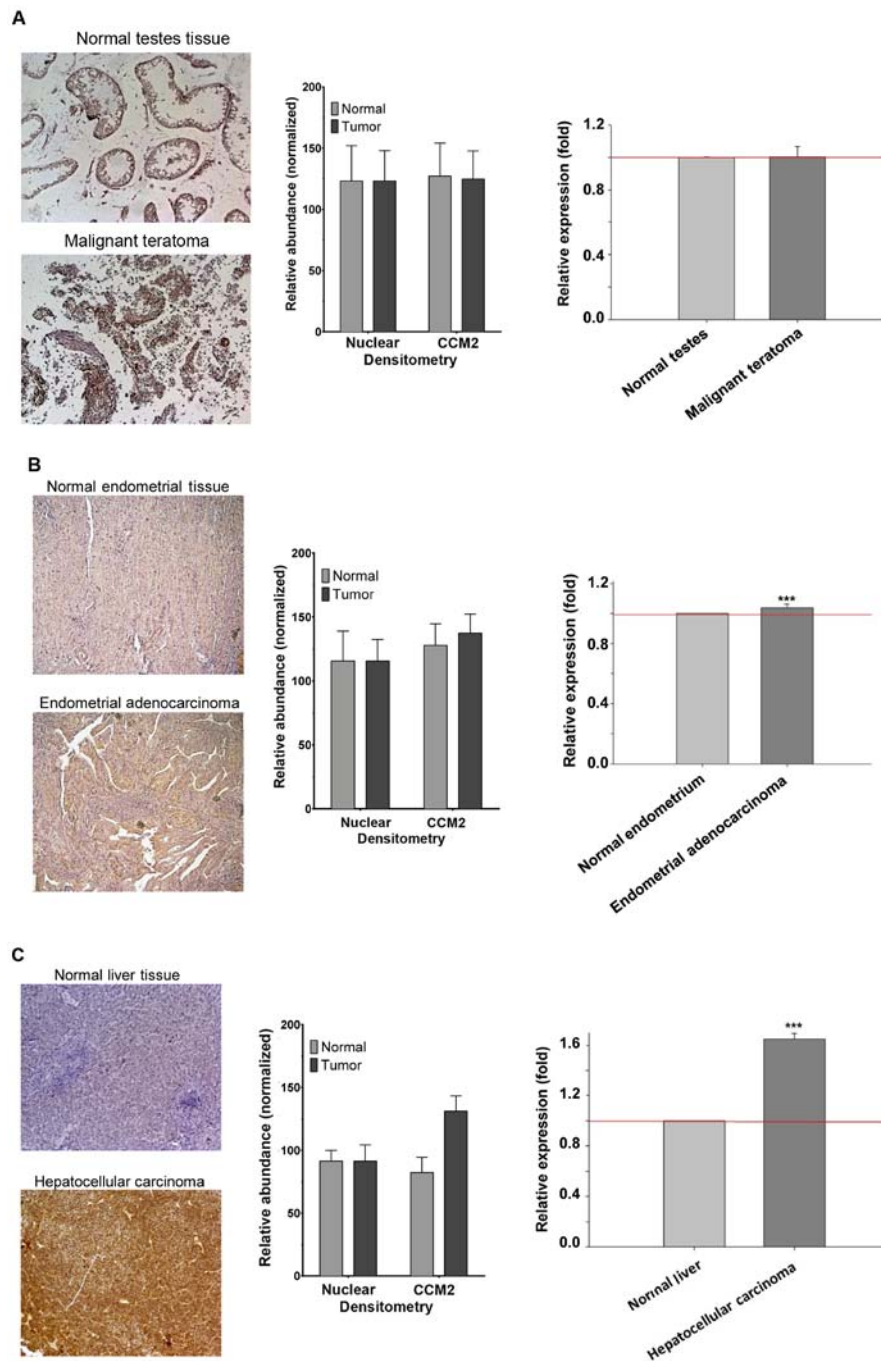


Figure 3. Altered expression of CCM2 protein associated with major human cancers. Additional paired-tissue samples, selected from testis, endometrium and liver, were acquired from different sources and vendors and further examined for comparative CCM2 protein expression with the CCM2 antibody utilizing immunohistochemistry (IHC) applications with horseradish peroxidase (HRP), 3,3'-diaminobenzidine (DAB) detection system and quantified with Elements Analysis software. The red/brown color from HRP/DAB reactivity with the CCM2 antibody was quantified and averaged between the red and green channel quantification and cell nuclei were quantified with the blue channel. Data were normalized against the respective internal controls using the blue channel for cell nuclei and background staining. Relative densitometry and relative expression of total CCM2 proteins are presented with bar plots where the light bars represent normal tissues (normal) and dark bars represent tumor tissues (tumor), among each tissue pair. (A) In testis paired-tissues, no statistical difference in the relative expression level of CCM2 between tumor (teratoma) and normal testis tissue for this pair was observed as shown in one selected tissue-pair (left panel) further confirmed with the quantification data (ROI, tumor=9,444; normal=16,306) (middle panel). The entire collection of paired samples was summarized as having no statistical difference (n=14, ROI range=7,362-18,137/sample) (right panel). (B) In the endometrial paired-tissues, a distinguishable difference in the relative intensity of CCM2 staining between tumor (endometrial adenocarcinoma) and normal endometrial tissues is presented by a selected tissue-pair (left panel), and the quantification of the relative expression level of CCM2 between the tumor (adenocarcinoma) and normal endometrial tissue for this pair showed marked differences (ROI, tumor=12,643; normal=12,114) (middle panel). Statistically significant increase in CCM2 proteins in the endometrial tumor were found from the entire collection of paired samples (n=12, ROI range=9,384-14,425/sample) (right panel) (** $P \leq 0.001$, for unpaired t-test). (C) In liver paired-tissues, a marked difference in the relative intensity of CCM2 staining between tumor (hepatocellular carcinoma) and normal liver tissues was visualized by a selected tissue-pair (left panel), and the quantification of the relative expression level of CCM2 between tumor (carcinoma) and normal liver tissue for this pair showed marked differences (ROI, tumor=11,078; normal=7,059, middle panel). Statistically significant increase of CCM2 proteins in liver tumor were found from the entire collection of paired samples (n=10, ROI range=3920-13319/sample) (right panel). The relative expression levels of endogenous CCM2 protein are presented with bar plots which was normalized against normal tissue cell nuclear staining among each tissue pair (middle panels) and further normalized against normal tissue for the entire collection (right panels) (** $P \leq 0.001$, for unpaired t-test). Red line on the quantification graphs represents baseline for the normalized control. CCM2, cerebral cavernous malformation 2; ROI, regions of interest.

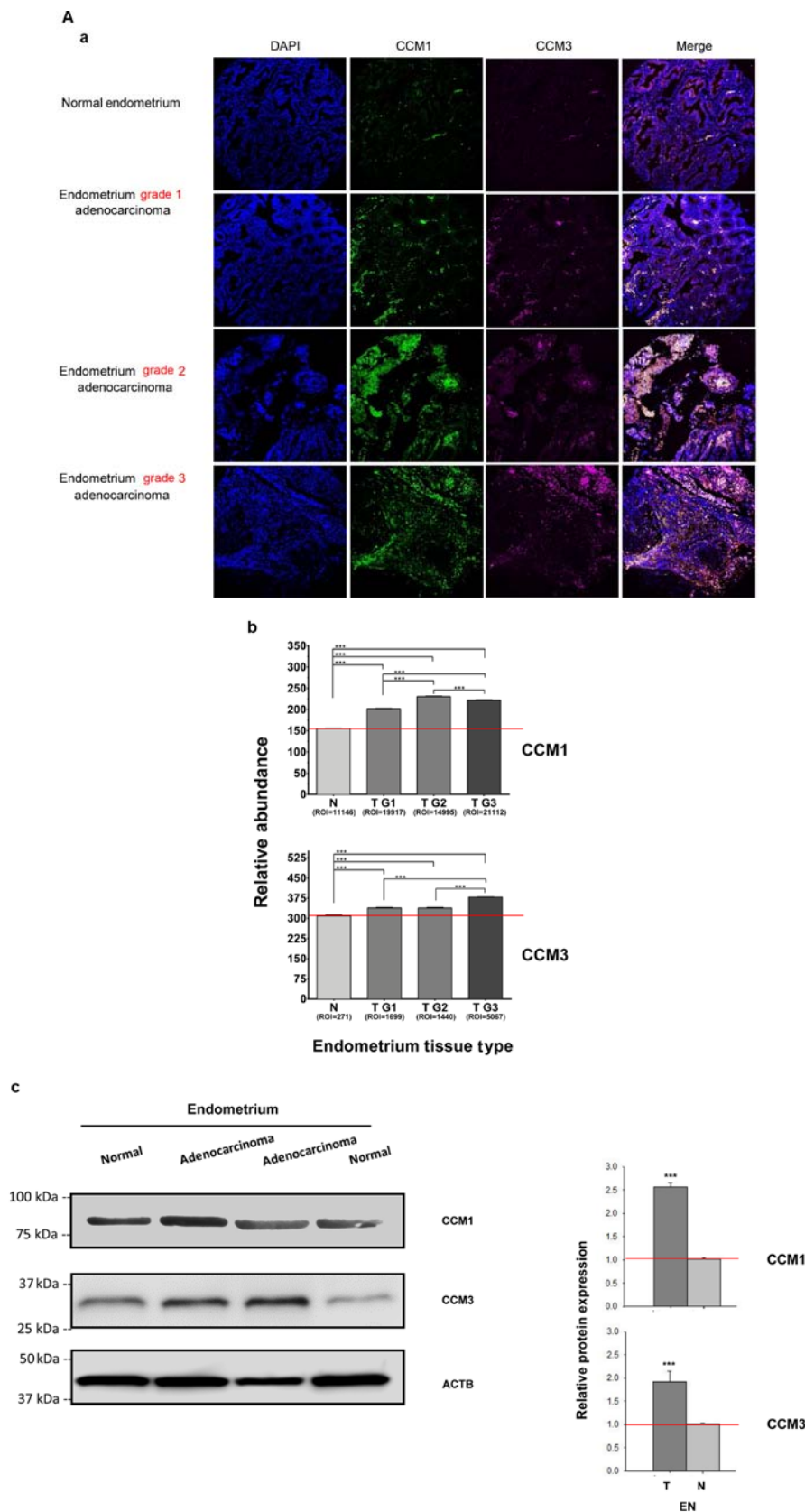


Figure 4. Significantly altered expression of CCM1 and CCM3 proteins in endometrial and liver cancers. The comparative CCM1 and CCM3 protein expression pattern was measured with immunofluorescence-labeled CCM1 and CCM3 antibodies, normalized against nuclear staining (DAPI), and quantified with Elements Analysis software. (A-a) The differential expression levels of CCM1 and CCM3 proteins in three different stages of endometrial tumor (adenocarcinoma, T), grade 1 (T G1), grade 2 (T G2), and grade 3 (T G3), compared to normal tissue (N) from paired endometrium samples, were visualized by multicolor immunofluorescence imaging. The correlation between the expression levels of CCM proteins and the specific stage of endometrial tumors was demonstrated through automated quantification of ROI intensities of CCM proteins and normalized against nuclear staining (DAPI). (b) Significant differences were observed through the quantification of the relative expression levels of CCM1 and CCM3 among the different stages of endometrial tumors (T, T G1, T G2, and T G3), compared to normal tissue (N). (c) Western blot analysis demonstrated increased expression levels of both CCM1 and CCM3 protein in endometrial (EN) tumor tissue (T) compared to normal tissue (N).

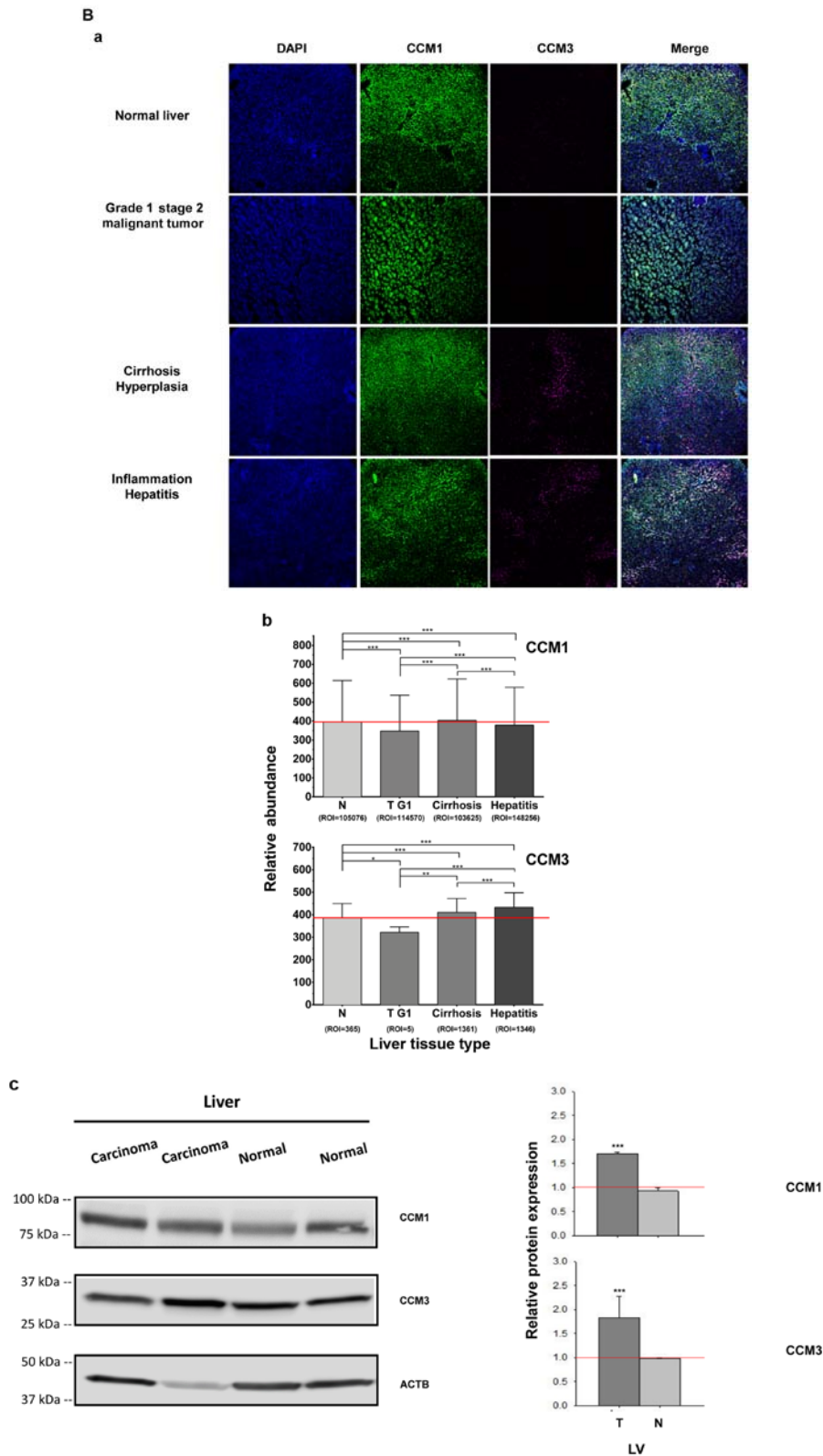


Figure 4. Continued. (B-a) Similarly, the differential expression levels of CCM1 and CCM3 proteins in different liver condition stages during tumorigenesis, hepatitis, cirrhosis and grade 1 stage 2 liver tumor tissue, compared to normal liver tissue from paired liver samples were visualized by multicolor immunofluorescence imaging. (b) The correlation between the expression levels of CCM proteins and the different liver conditions was demonstrated through automated quantification of ROI intensities of CCM proteins and normalized against nuclear staining (DAPI). The significant differences were observed through the quantification of the relative expression levels of CCM1 and CCM3 among different liver conditions (hepatitis, cirrhosis, and T G1), compared to normal tissue (N). (c) Western blot analysis demonstrated increased expression levels of both CCM1 and CCM3 proteins in liver (LV) tumor (T) compared to normal tissue (N). Automated quantification of ROI intensities of CCM proteins in IF images was accomplished with Elements Analysis software accompanying Nikon EclipseTi confocal microscope. The graph is a representative quantification obtained of the three different experiments among 97 paired samples. For statistical analysis, *** $P \leq 0.001$, ** $P \leq 0.01$ and * $P \leq 0.05$, respectively, for unpaired t-test, ROI=5-148,256, depending on tissue sample and fluorescence channel being quantified. The quantification of the relative expression levels of CCM1 and CCM3 proteins in the western blot analysis was measured through quantification of band intensities of CCM1 and CCM3 proteins from four different experiments and normalized against β -actin (ACTB). For statistical analysis, *** $P \leq 0.001$ indicates the significant increase in CCM1 and CCM3 proteins. Red line on the quantification graphs represents baseline for the normalized control. CCM, cerebral cavernous malformation; ROI, regions of interest.

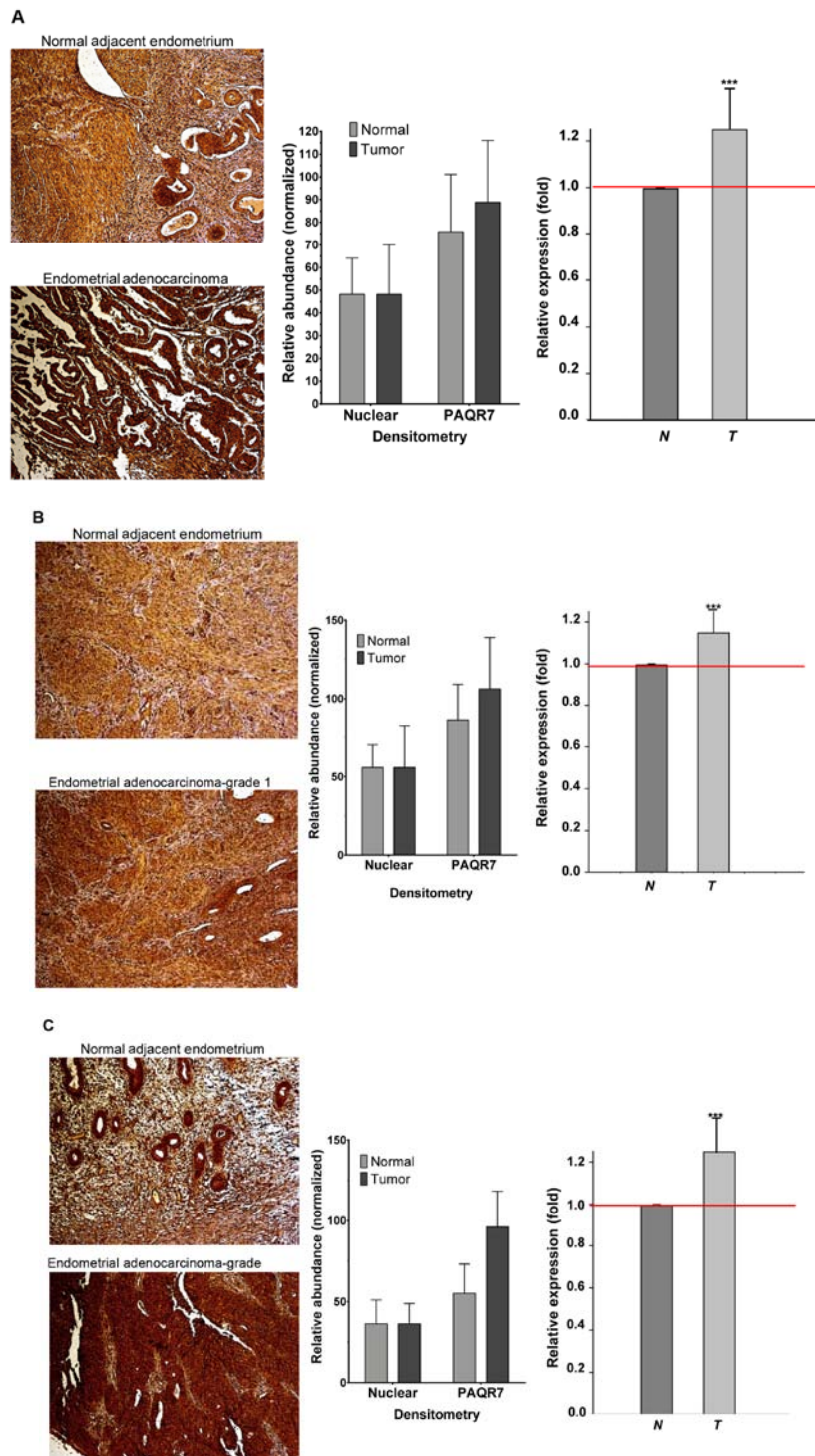


Figure 5. Altered expression of PAQR7 protein in endometrial and liver cancers. Additional paired-tissue samples from both endometrium and liver were acquired and further examined for comparative PAQR7 protein expression patterns with PAQR7 antibody utilizing immunohistochemistry (IHC) applications with horseradish peroxidase (HRP), 3,3'-diaminobenzidine (DAB) detection system and quantified with Elements Analysis software. The red/brown color from HRP/DAB reactivity with the PAQR7 antibody was quantified and averaged between the red and green channel quantification and cell nuclei were quantified with the blue channel. Data were normalized against the respective internal controls using the blue channel for cell nuclei and background staining. Relative densitometry and relative expression of total PAQR7 proteins are presented with bar plots where the dark bars represent normal tissues (N) and light bars represented tumor tissues (T), among each tissue pair. (A) In the endometrial paired-tissues, a distinguishable difference in the relative intensity of PAQR7 staining between tumor (endometrial adenocarcinoma) and normal endometrial tissues is presented from a selected tissue-pair (left panel), and the quantification of the relative expression level of PAQR7 for this tissue-pair showed marked differences (ROI, tumor=50,451; normal=21,400) (middle panel). Statistically significant increase in PAQR7 protein in endometrial tumors was found from the entire collection of paired samples (n=12, ROI range=12,305-77,227/sample) (right panel). (B) Among the different grades of endometrial adenocarcinoma, a visual enhancement in the relative intensity of PAQR7 staining in grade 1 endometrial adenocarcinoma is presented from a selected tissue-pair (left panel), and the quantification of the relative expression level of PAQR7 for this tissue-pair showed vast differences (ROI, tumor=18,266; normal= 21,158) (middle panel). Statistically significant increase in PAQR7 protein in the endometrial tumor was found from the entire collection of grade 1 paired samples (n=6, ROI range=12,305-77,227/sample) (right panel). (C) A significant increase in the relative intensity of PAQR7 staining in grade 2-3 endometrial adenocarcinoma is presented in a selected tissue-pair (left panel), and the quantification of the relative expression level of PAQR7 for this tissue-pair showed major differences (ROI, tumor=77,227; normal= 35,832) (middle panel). Statistically significant increase in PAQR7 protein in the endometrial tumor was found in the entire collection of grade 2-3 paired samples (n=4, ROI range=29,095-77,227/sample) (right panel).

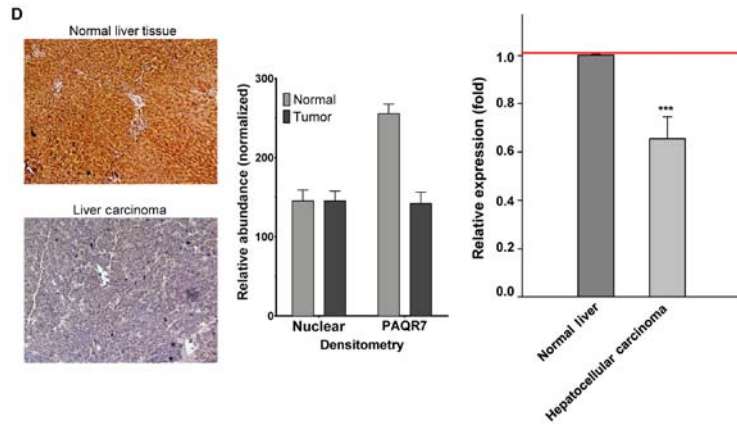


Figure 5. Continued. (D) In liver paired-tissues, the relative intensity of PAQR7 staining between tumor (hepatocellular carcinoma) and normal liver tissues is visualized in a selected tissue-pair (left panel), and the quantification of the relative expression level of PAQR7 between tumor (carcinoma) and normal liver tissue for this pair showed a marked decrease (ROI, tumor=10,219; normal=16,166) (middle panel). Statistically significant decrease in the PAQR7 protein in liver tumor was found in the entire collection of paired samples (n=16, ROI=10,219-16,166/sample) (right panel). All data from the entire collections (n>10) were normalized by normal tissue among each tissue pair (**P<0.001 for unpaired t-test). Red line on the quantification graphs represents baseline for the normalized control. PAQR7, progesterin and adipoQ receptor 7; ROI, regions of interest.

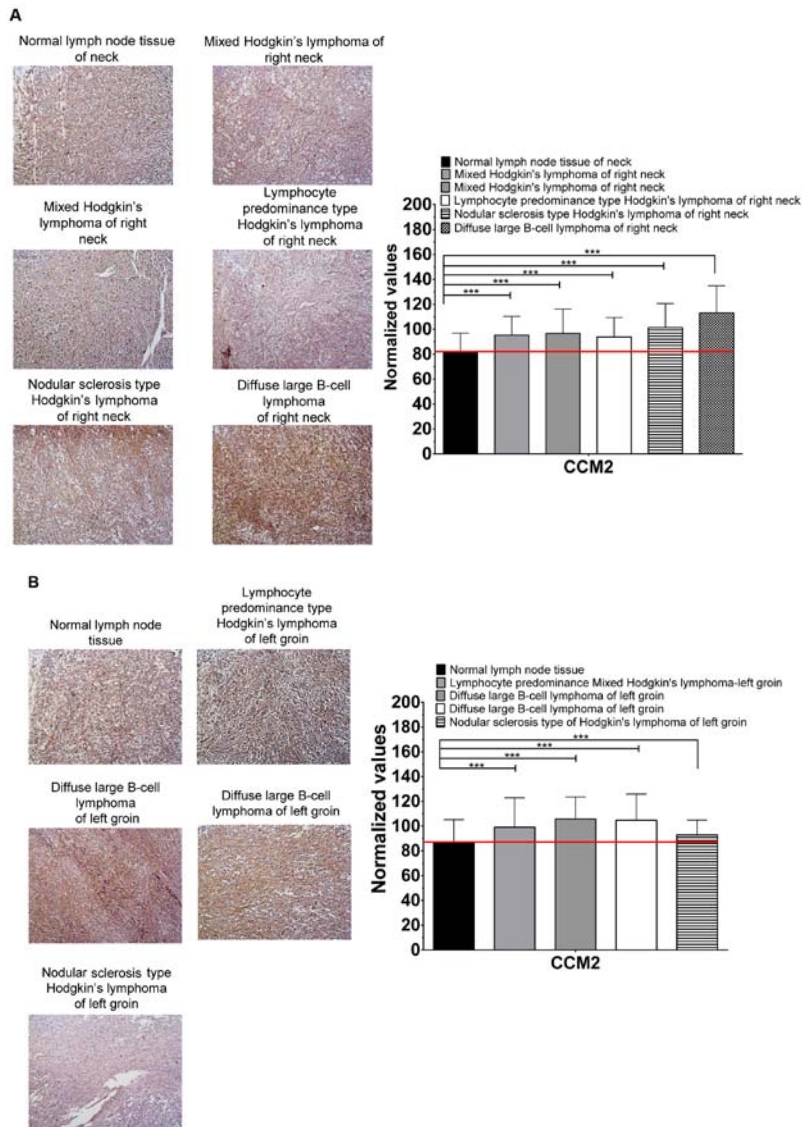


Figure 6. Significantly increased protein expression of CCM2 in heterogeneous lymphatic cancers. The significantly increased expression of CCM2 protein in tumor tissue (myeloma or lymphoma) (detailed in each panel), compared to adjacent normal lymph node from tumor tissue sections, from the (A) neck, (B) groin, (C) clavicle and sternum, (D) B-cell lymphoma of various organs and (E) T-cell lymphoma of various organs was assessed utilizing immunohistochemistry (IHC) applications with horseradish peroxidase (HRP), 3,3'-diaminobenzidine (DAB) detection system and quantified with Elements Analysis software.

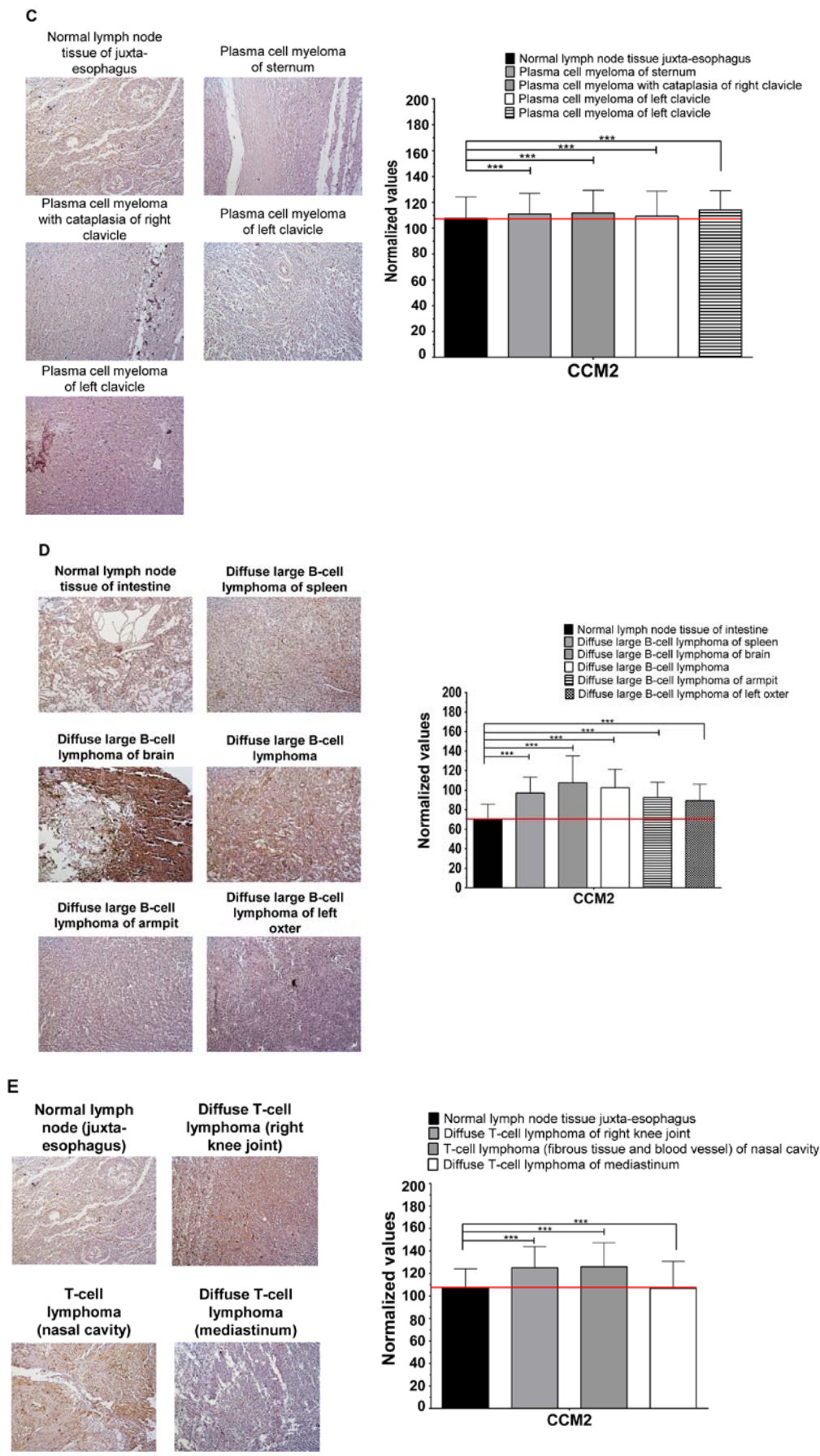


Figure 6. Continued. The significantly increased expression of CCM2 protein in tumor tissue (myeloma or lymphoma) (detailed in each panel), compared to adjacent normal lymph node from tumor tissue sections, from the (A) neck, (B) groin, (C) clavicle and sternum, (D) B-cell lymphoma of various organs and (E) T-cell lymphoma of various organs was assessed utilizing immunohistochemistry (IHC) applications with horseradish peroxidase (HRP), 3,3'-diaminobenzidine (DAB) detection system and quantified with Elements Analysis software.

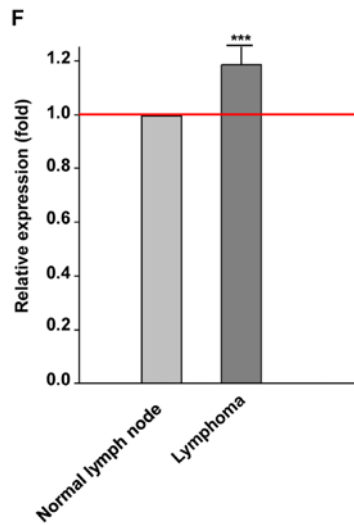


Figure 6. Continued. (F) Collectively, all lymphomas were quantified demonstrating statistically increased expression of CCM2 among various lymphomas. (A) The visual difference in the relative intensity of CCM2 staining, among various lymphomas and normal lymph node in the neck was observed with DAB staining (left panel); significant differences were confirmed through the quantification of the relative expression level of CCM2 between each lymphoma and normal lymph node (right panel). (B) A significant difference in the relative intensity of CCM2 staining was observed among various lymphomas and normal lymph node in the groin (left panel); and significant differences were observed through the quantification of the relative expression level of CCM2 between each lymphoma and normal lymph node (right panel). (C) Significant visual differences in the relative intensity of CCM2 staining among plasma cell myeloma and normal lymph node was observed in the clavicle and sternum (left panel); and significant differences were determined through the quantification of the relative expression level of CCM2 between each myeloma and normal lymph node (right panel). (D) Significant differences in the relative intensity of CCM2 staining among B-cell lymphomas and normal lymph node can be generalized in various tissues (left panel); and significant differences were assessed through the quantification of the relative expression level of CCM2 between each lymphoma and normal lymph node (right panel). (E) Significant visual differences in the relative intensity of CCM2 staining among T-cell lymphomas, in the knee, nasal cavity and mediastinum, and normal lymph node were observed (left panel); and significant differences were confirmed through the quantification of the relative expression level of CCM2 between each T-cell lymphoma and normal lymph node (right panel). (F) Statistically significant increases in CCM2 proteins were found among almost all lymphomas examined and generalized with the entire collection of lymphoma samples (n=43). The red/brown color from HRP/DAB reactivity with the CCM2 antibody was quantified and averaged between the red and green channel quantification and cell nuclei were quantified with the blue channel. Data were normalized against the respective control using the blue channel for cell nuclei and background staining. Automated quantification of ROI intensities of CCM2 proteins was accomplished with Elements Analysis software. The graph is a representative quantification obtained of the different experiments ($^{***}P \leq 0.001$ for unpaired t-test, ROI=6,443-16,587, depending on tissue sample). The red line on the quantification graphs represents baseline for the normalized control. CCM2, cerebral cavernous malformation 2.

elucidate the underlying relationship and mechanisms among CCM1 and CCM3 to further understand the role of the CSC during tumorigenesis.

Discussion

This is the first report to systematically examine the altered expression patterns of cerebral cavernous malformation (CCM) proteins in various human cancers and delineate

certain expression patterns of CCMs associated with specific cancer types and the severity of certain cancers. Our results implicate the future potential application of CCM proteins for clinical diagnosis and prognosis. In oncology, biomarkers can be used for risk assessment of treatment, prediction of response to treatment, drug screening, determination of differential diagnosis and prognosis, and monitoring of the progression of disease. For patients diagnosed with a cancer, biomarkers can help determine the likelihood of disease recurrence independent of treatment, suggesting the use of biomarkers as one of the most valuable tools for cancer therapy.

Our recent research demonstrated the existence of multiple isoforms of the CCM2 protein, further indicating the complexity of the CCM signaling complex (CSC) (11). However, we found that almost all expressed CCM2 isoforms are ubiquitously expressed in various cells and tissues, indicating their potential involvement in diverse cellular events during biogenesis. Furthermore, our findings that CCM2 isoforms were differentially expressed among various tissues and cells, at both the transcriptional and translational levels, suggest an important role of CCM2 in various cancers during tumorigenesis, and widen our current view concerning the cellular functions played by CCM2 (11). CCM2 (isoform 100) has been suggested for its role as a possible potent angiogenic factor (15) and was observed to have increased RNA expression in liver cancer tissues, while displaying the opposite trend in endometrial cancers, suggesting various roles of this isoform in tumorigenesis. This observation was further supported with altered expression of another CCM2 isoform (CCM2-212) in various types of cancer. Despite the heterogeneity among various lymphomas, a clear increased expression of total CCM2 was observed for more than 43 lymphoma samples from various locations and cancer subtypes. Based on our findings, we propose that the differential expression pattern of CCM2 has great potential in aiding the diagnosis of various types of cancer.

Our data also suggest that expression patterns of CCM1 and CCM3 can also be used to delineate various stages of endometrial cancers and early stages of tumorigenesis in liver cancers. To validate CCM1 and CCM3 as biomarker candidates, we were able to demonstrate a parallel trend of increased expression of the traditional endometrial cancer marker, PAQR7, with increasing grades of endometrial cancer, but observed the opposite trend of PAQR7 in liver cancers, suggesting multiple coordinated roles of the CSC complex and PAQR7 across various cancers. In conclusion, the tumor-specific CCM expression patterns, we defined in this investigation, may have great potential clinical applications in future cancer diagnosis and prognosis. This project also provides new insights into the CSC-mediated signaling pathways in tumorigenesis, which may revolutionize the current concepts of the CSC-mediated signaling and molecular mechanisms of tumorigenesis, leading to new therapeutic strategies.

Acknowledgements

We wish to thank Kamran Falahati, Akhil Padarti, Nancy Jiang, Khalid Shoukat, Deepak Muthyala, Shen Sheng,

Ahmed Badr, Junli Zhang, Amna Siddiqui, Saafan Malik, and Edna Lopez at Texas Tech University Health Science Center El Paso (TTUHSCEP) for their technical help during the experiments.

Funding

This research study was supported and funded by the Coldwell Foundation and Texas Tech University Health Science Center El Paso (TTUHSCEP) (JZ).

Availability of data and materials

The datasets used during the present study are available from the corresponding author upon reasonable request.

Authors' contributions

JZ, JAF, YQ, EMG and MS performed all of the experiments. JZ and JAF analyzed the data; JZ. and JAF contributed to draft materials and wrote the manuscript. All authors read and approved the manuscript and agree to be accountable for all aspects of the research in ensuring that the accuracy or integrity of any part of the work are appropriately investigated and resolved.

Ethics approval and consent to participate

All tissue slides were purchased and collected under the highest ethical standards with the donor being informed completely and with their consent. The vendors guarantee to follow standard medical care and protect the donors' privacy. All human tissues were collected under HIPPA approved protocols. All samples were tested negative for HIV and hepatitis B or their counterparts in animals, and approved for commercial product development. IRB ethical approval was waived since IRB review is not required for laboratory research on de-identified human cell lines or human tissue obtained from commercial or governmental entities, as the release of these samples to investigators does not meet the regulatory definition of human subject research.

Patient consent for publication

Not applicable.

Competing interests

The authors declare that no competing interests exist.

References

- Zhang J, Clatterbuck RE, Rigamonti D, Chang DD and Dietz HC: Novel insights regarding the pathogenesis of cerebral cavernous malformation (CCM). *Am J Hum Genet* 69: 178, 2001.
- Zhang J, Basu S, Rigamonti D, Dietz HC and Clatterbuck RE: Krit1 modulates beta 1-integrin-mediated endothelial cell proliferation. *Neurosurgery* 63: 571-578, discussion 578, 2008.
- Zhang J: Molecular biology of cerebral cavernous malformation. In: *Cavernous Malformations of the Nervous System*. Rigamonti D (ed). Cambridge University Press, New York, NY, pp31-40, 2011.
- Zhang J, Carr C and Badr A: The cardiovascular triad of dysfunctional angiogenesis. *Transl Stroke Res* 2: 339-345, 2011.
- Zhang J, Dubey P, Padarti A, Zhang A, Patel R, Patel V, Cistola D and Badr A: Novel functions of CCM1 delimit the relationship of PTB/PH domains. *Biochim Biophys Acta Proteins Proteomics* 1865: 1274-1286, 2017.
- Padarti A and Zhang J: Recent advances in cerebral cavernous malformation research. *Vessel Plus* 2: 21, 2018.
- Ma X, Zhao H, Shan J, Long F, Chen Y, Chen Y, Zhang Y, Han X and Ma D: PDCD10 interacts with Ste20-related kinase MST4 to promote cell growth and transformation via modulation of the ERK pathway. *Mol Biol Cell* 18: 1965-1978, 2007.
- Hilder TL, Malone MH, Bencharit S, Colicelli J, Haystead TA, Johnson GL and Wu CC: Proteomic identification of the cerebral cavernous malformation signaling complex. *J Proteome Res* 6: 4343-4355, 2007.
- Voss K, Stahl S, Schleider E, Ullrich S, Nickel J, Mueller TD and Felbor U: CCM3 interacts with CCM2 indicating common pathogenesis for cerebral cavernous malformations. *Neurogenetics* 8: 249-256, 2007.
- Zhang J, Clatterbuck RE, Rigamonti D and Dietz HC: Cloning of the murine Krit1 cDNA reveals novel mammalian 5' coding exons. *Genomics* 70: 392-395, 2000.
- Jiang X, Padarti A, Qu Y, Sheng S, Abou-Fadel J, Badr A and Zhang J: Alternatively spliced isoforms reveal a novel type of PTB domain in CCM2 protein. *Sci Rep* 9: 15808, 2019.
- Orso F, Balzac F, Marino M, Lembo A, Retta SF and Taverna D: miR-21 coordinates tumor growth and modulates KRIT1 levels. *Biochem Biophys Res Commun* 438: 90-96, 2013.
- Pan X, Wang ZX and Wang R: MicroRNA-21: A novel therapeutic target in human cancer. *Cancer Biol Ther* 10: 1224-1232, 2010.
- Glading AJ and Ginsberg MH: Rap1 and its effector KRIT1/CCM1 regulate beta-catenin signaling. *Dis Model Mech* 3: 73-83, 2010.
- Chan AC, Li DY, Berg MJ and Whitehead KJ: Recent insights into cerebral cavernous malformations: Animal models of CCM and the human phenotype. *FEBS J* 277: 1076-1083, 2010.
- Harel L, Costa B, Tcherpakov M, Zapatka M, Oberthuer A, Hansford LM, Vojvodic M, Levy Z, Chen ZY, Lee FS, *et al*: CCM2 mediates death signaling by the TrkA receptor tyrosine kinase. *Neuron* 63: 585-591, 2009.
- Gruber-Olipitz M and Segal RA: Live or let die: CCM2 provides the link. *Neuron* 63: 559-560, 2009.
- Lambertz N, El Hindy N, Kreitschmann-Andermahr I, Stein KP, Dammann P, Oezkan N, Mueller O, Sure U and Zhu Y: Downregulation of programmed cell death 10 is associated with tumor cell proliferation, hyperangiogenesis and peritumoral edema in human glioblastoma. *BMC Cancer* 15: 759, 2015.
- Nickel AC, Wan XY, Saban DV, Weng YL, Zhang S, Keyvani K, Sure U and Zhu Y: Loss of programmed cell death 10 activates tumor cells and leads to temozolomide-resistance in glioblastoma. *J Neurooncol* 141: 31-41, 2019.
- Zhu Y, Zhao K, Prinz A, Keyvani K, Lambertz N, Kreitschmann-Andermahr I, Lei T and Sure U: Loss of endothelial programmed cell death 10 activates glioblastoma cells and promotes tumor growth. *Neuro-oncol* 18: 538-548, 2016.
- Fu X, Zhang W, Su Y, Lu L, Wang D and Wang H: MicroRNA-103 suppresses tumor cell proliferation by targeting PDCD10 in prostate cancer. *Prostate* 76: 543-551, 2016.
- Geng L, Sun B, Gao B, Wang Z, Quan C, Wei F and Fang XD: MicroRNA-103 promotes colorectal cancer by targeting tumor suppressor DICER and PTEN. *Int J Mol Sci* 15: 8458-8472, 2014.
- Xiong B, Lei X, Zhang L and Fu J: miR-103 regulates triple negative breast cancer cells migration and invasion through targeting olfactomedin 4. *Biomed Pharmacother* 89: 1401-1408, 2017.
- Kfir-Erenfeld S, Haggiag N, Biton M, Stepensky P, Assayag-Asherie N and Yefenof E: miR-103 inhibits proliferation and sensitizes hemopoietic tumor cells for glucocorticoid-induced apoptosis. *Oncotarget* 8: 472-489, 2017.
- Garofalo M, Romano G, Di Leva G, Nuovo G, Jeon YJ, Ngankeu A, Sun J, Lovat F, Alder H, Condorelli G, *et al*: EGFR and MET receptor tyrosine kinase-altered microRNA expression induces tumorigenesis and gefitinib resistance in lung cancers. *Nat Med* 18: 74-82, 2011.

26. Yang D, Wang JJ, Li JS and Xu QY: miR-103 functions as a tumor suppressor by directly targeting programmed cell death 10 in NSCLC. *Oncol Res* 26: 519-528, 2018.
27. Livak KJ and Schmittgen TD: Analysis of relative gene expression data using real-time quantitative PCR and the 2^{-Delta Delta C(T)} Method. *Methods* 25: 402-408, 2001.
28. Dressing GE, Goldberg JE, Charles NJ, Schwertfeger KL and Lange CA: Membrane progesterone receptor expression in mammalian tissues: A review of regulation and physiological implications. *Steroids* 76: 11-17, 2011.
29. Charles NJ, Thomas P and Lange CA: Expression of membrane progesterone receptors (mPR/PAQR) in ovarian cancer cells: Implications for progesterone-induced signaling events. *Horm Cancer* 1: 167-176, 2010.
30. Romero-Sánchez M, Peiper SC, Evans B, Wang Z, Catasús L, Ribe A, Prat J and Giri JG: Expression profile of heptahelical putative membrane progesterone receptors in epithelial ovarian tumors. *Hum Pathol* 39: 1026-1033, 2008.



This work is licensed under a Creative Commons Attribution-NonCommercial-NoDerivatives 4.0 International (CC BY-NC-ND 4.0) License.